Manuscript prepared for Atmos. Chem. Phys.
with version 3.2 of the LaTeX class copernicus.cls.
Date: 29 March 2011

Supplement to photochemical modeling of glyoxal at a rural site: observations and analysis from BEARPEX 2007

A. J. Huisman[1,11], J. R. Hottle[1,2], M. M. Galloway[1], J. P. DiGangi[1], K. L. Coens[1], W. S. Choi[3], I. C. Faloona[3], J. B. Gilman[4], W. C. Kuster[4], J. de Gouw[4], N. C. Bouvier-Brown[5], A. H. Goldstein[5], B. W. LaFranchi[6], R. C. Cohen[6], G. M. Wolfe[1], J. A. Thornton[7], K. S. Docherty[8,9], D. K. Farmer[8], M. J. Cubison[8], J. L. Jimenez[8], J. Mao[10], W. H. Brune[10], and F. N. Keutsch[1]

[1]Dept. of Chemistry, University of Wisconsin-Madison, Madison, WI, USA
[2]Current Address: Air Force Office of Scientific Research–Physics and Electronics Directorate, Arlington, VA, USA
[3]Dept. of Land, Air, and Water Resources, University of California-Davis, Davis, California, USA
[4]NOAA Earth System Research Laboratory and Cooperative Institute for Research in Environmental Sciences, University of Colorado, Boulder, CO, USA
[5]Dept. of Environmental Science, Policy, and Management, University of California, Berkeley, CA, USA
[6]Dept. of Chemistry, University of California, Berkeley, CA, USA
[7]Dept. of Chemistry, University of Washington, Seattle, WA, USA
[8]CIRES and Dept. of Chemistry and Biochemistry, Univ. of Colorado, Boulder, CO, USA
[9]Currently at Alion Science and Technology, EPA Office of Research and Development, Research Triangle Park, NC, USA
[10]Dept. of Meteorology, Pennsylvania State University, University Park, Pennsylvania, USA
[11]Institute for Atmospheric and Climate Science, ETH Zurich, Zurich, Switzerland

Correspondence to: F. Keutsch keutsch@chem.wisc.edu

1 Supplement

1.1 Other measurement techniques

Measurements of meteorological parameters were made consistent with the AmeriFlux Network (Goldstein et al., 2000), including wind speed and direction, air temperature, humidity, and ozone concentration.

A gas chromatograph with quadrupole mass spectrometer (GC-MS) instrument was optimized to quantify C_{10} – C_{15} biogenic compounds (including methyl chavicol) as described in detail by Bouvier-Brown et al. (2009). One inlet was located 1.5 m above the forest floor, below the main trees of the canopy but near the juvenile saplings, from 19 August through the morning of 12 September (DOY 231–255). The other inlet was located 9.3 m above the forest floor, which corresponds to 2 m above the mean forest canopy height, from the afternoon of 12 September through 8 October (DOY 255–281).

C_2 – C_{10} organic compounds were quantified in situ using a gas chromatograph with mass spectrometric detection (GC-MS). The sample acquisition procedure is described in detail by Goldan

et al. (2004) with more recent modifications to the analysis system given in Gilman et al. (2010).

Speciated acyl peroxy nitrate (APN) measurements were obtained via a custom thermal dissociation – chemical ionization mass spectrometer (TD–CIMS), as described by Wolfe et al. (2009). We used data from level one (1.5 m) of the APN instrument for this analysis. Using data from the other levels results in only minor differences in correlation coefficients and fitting parameters and would not impact the conclusions drawn here.

Measurements of OH and HO_2 were obtained by a Laser Induced Fluorescence (LIF) system as described by Faloona et al. (2004), and measurements of NO_2 were obtained by a separate thermal dissociation–LIF system similar to the one described in Day et al. (2002).

An Aerodyne high-resolution time-of-flight aerosol mass spectrometer (HR-ToF-AMS; DeCarlo et al. (2006)) was used to monitor submicron non-refractory aerosol concentration and composition from an inlet located above the canopy. Further details on the AMS operation during BEARPEX 2007 can be found in Farmer et al. (2010). Oxygenated organic aerosol (OOA, an SOA surrogate) and hydrocarbon-like organic aerosol (HOA, a surrogate for combustion primary OA) were derived from positive matrix factorization of the AMS spectra (Ulbrich et al., 2009), with the large majority of the organic aerosol at the site being OOA. Aerosol surface area was estimated from the number particle size distributions measured with a scanning mobility particle sizer (SMPS, TSI Model 3081, St. Paul, MN) assuming particle sphericity.

The observations of boundary layer height were determined by investigation of temperature, humidity, and wind profiles obtained with a tethersonde during BEARPEX 2007 (Choi et al., 2010).

1.2 Modifications to MCM for 0–D photochemical model

1.2.1 Dry deposition

Dry deposition was included by appending a term of form $-V_{dep}\times$[X]/BL to the differential equation for a given molecule, where V_{dep} is the dry deposition velocity of species X and BL is the height of the boundary layer. An assumed, parameterized boundary layer which varied between 100–800 m (Dillon et al., 2002; Wolfe et al., 2009; Choi et al., 2010) with a functional form tied to the rate constant for NO_2 photolysis was used. The parameterized boundary layer matches reasonably with measurements (Choi et al., 2010) from the site (which were available during the daytime only), as shown in Fig. S1. The parameterization was made before measurements of BL height were available, but the model results for glyoxal change by less than 1% when using the correct peak BL height. This is probably because deposition is least effective during the day and the change from 800 m to 700 m peak BL is proportionally small.

Depositions were added to all molecules which had Simplified Molecular Input Line Entry Specification (SMILES) strings indicating that they were alcohols or peroxides (V_{dep} = 0.3 $cm\,s^{-1}$), peroxy acyl nitrates (V_{dep} = 0.84 $cm\,s^{-1}$) (Farmer and Cohen, 2008), alkyl nitrates (V_{dep} = 2.10

$\mathrm{cm\ s^{-1}}$) (Farmer and Cohen, 2008), and for the specific species O_3 (V_{dep} = 0.08 $\mathrm{cm\ s^{-1}}$) (LaFranchi, 2008), HNO_3 (V_{dep} = 2.5 $\mathrm{cm\ s^{-1}}$) (Farmer and Cohen, 2008), and glyoxal (V_{dep} = 0.3 $\mathrm{cm\ s^{-1}}$) (Volkamer et al., 2007). In the event that a multifunctional compound was tagged with more than one deposition rate, only the highest rate was retained.

1.2.2 Gas–to–aerosol partitioning of glyoxal

Loss of gas phase glyoxal to the aerosol phase was treated following Volkamer et al. (2007) by appending a term $-k_{AERGLY} \times SA \times$[glyoxal] to the differential equation for glyoxal, where k_{AERGLY} = $\gamma \times k$ is the aerosol loss rate constant. k_{AERGLY} was calculated using the effective uptake coefficient $\gamma = 0.0037$ from Volkamer for Mexico City, k=8.5×10^{-5} to convert to units of $\mathrm{s^{-1}}$, and SA is the surface area of aerosol in $\mathrm{mm^2\ m^{-3}}$ at BEARPEX 2007. Analysis of the ratio of modeled to measured glyoxal for model runs without an aerosol sink term show that aerosol loss did not contribute substantially to the model overprediction during BEARPEX 2007, see Fig. S2.

1.2.3 Methyl chavicol degradation chemistry

A recent publication showed that methyl chavicol, a biogenic VOC, was present at BEARPEX 2007 in considerable mixing ratios (average daily peak concentration $>$0.4 $\mathrm{ppb_v}$) (Bouvier-Brown et al., 2009). Methyl chavicol forms glycolaldehyde, a major precursor for glyoxal, upon oxidation by OH with a yield estimated to be 37 $\pm$ 5% (Lee et al., 2006), reacting through the scheme depicted in Fig. S3. This chemistry was approximated for use in the model by examining the reactions of methyl chavicol (Bouvier-Brown et al., 2009) and searching for analogs of the products which were already included in the MCM, Fig. S4. In general, the MCM analogs are missing a methyl ether group but are otherwise structurally similar to the actual products. No attempt was made to correct the carbon balance by producing additional smaller fragments; the rate constants and branching ratios were also unaltered. Although these compounds will not have chemistry which is identical to those of the methyl chavicol reaction products, this simplified treatment allows some insight into their possible influence on glyoxal. Methyl chavicol may prove to be an important source of glyoxal because it has the potential for fast (second–generation via glycolaldehyde) in addition to higher–generation (ex. ring opening) production.

1.2.4 Adjusted OH + MPAN rate constant

The rate constant for OH + MPAN was adjusted in accordance with Orlando et al. (2002) to k=3.2×10^{-11} $\mathrm{cm^3\ molecule^{-1}\ s^{-1}}$.

1.2.5 Dilution

A diurnal dilution factor tied to the boundary layer height (see above) was included, with maximum value given by the average of reported dilution rate constant from Perez et al. (2009). This term was

added by appending $-\mathrm{k_{dil}}\times$[X] to the end of each molecule's differential equation, with $\mathrm{k_{dil}}$ varying from $0 - 8.75\times10^{-5}\ \mathrm{s^{-1}}$ over the course of a day. For simplicity, the background concentration into which the box mixed was assumed to have a concentration of zero for all gasses. We acknowledge that in reality, dilution is unlikely to be exactly zero at night. However, the ability of the model to correctly predict the net loss rate at night (see deposition, above) suggests that nighttime dilution is not a dominant process and that this parameterization of dilution is correct to a first approximation. Attempts to bring modeled glyoxal into agreement with measurement by scaling up the dilution rate were unsuccessful, as they resulted in an inverted diurnal profile due to the resulting very high dilution rates at mid–day.

1.2.6 Altered MBOAO2 chemistry

The model prediction of OVOC chemistry is shown for several compounds in Fig. 6. In particular, the agreement of model to measurement for MVK is better than the agreement for glyoxal. In the model, glycolaldehyde is overwhelmingly a product of MBO oxidation by OH, while MVK is a product of isoprene oxidation, so it is natural to examine the chemistry which links MBO to glycolaldehyde via MBOAO2 when seeking to explain the over–prediction in glyoxal. One possibility is that the chemical reactions of MBOAO2 in the MCM are incorrect at lower–$\mathrm{NO_x}$, although the model was able to reproduce both high and low–$\mathrm{NO_x}$ chamber studies of MBO oxidation very well. However, a test calculation predicted a total $\mathrm{RO_2}$ / $\mathrm{HO_2}$ ratio of over 20 just after initiation of chamber oxidation (Galloway et al., 2011), while the model of ambient conditions at BFRS typically had total $\mathrm{RO_2}$ / $\mathrm{HO_2} < 2$. Thus, reactions of MBOAO2 with $\mathrm{HO_2}$ could be hard to discern in the chamber study.

A model sensitivity analysis was thus performed to determine the magnitude of change in the $\mathrm{HO_2}$ + MBOAO2 reaction which would be required to bring modeled glyoxal into agreement with measurement. The product of the $\mathrm{HO_2}$+ MBOAO2 reaction, MBOAOOH, forms glycolaldehyde only as a minor product with about 10% yield via reaction with OH to return to MBOAO2 or photolysis to yield MBOAO which rapidly forms glycolaldehyde. Thus an increase in the formation of MBOAOOH would generally reduce the formation of glycolaldehyde and thus glyoxal. The results of this analysis (AB+ basis, $\mathrm{HO_2}$ driven to match measurement), Fig. S8, show that the rate constant for the MBOAO2 + $\mathrm{HO_2}$ must be increased by a factor of $\sim$65 to yield approximately the correct noontime glyoxal. In the top panel, the model over–prediction at noon and 0.65 day is plotted as a function of the enhancement of the MBOAO2 + $\mathrm{HO_2}$ rate constant, with associated power–law fits. The bottom panel shows the diurnal profile of modeled and measured glyoxal, with lines indicating the two points in time where ratios were taken. An increase in rate constant of this magnitude is not possible for a number of reasons, including especially that it exceeds the gas kinetic rate.

1.2.7 Reduced yield of glyoxal from glycolaldehyde

Because the model was able to perform adequately in chamber experiments, global modifications to chemistry are less apt than changes targeted directly to the chemistry of glyoxal. For example, a model run which reduced all $\mathrm{RO_2}$ by including a temporally invariant pseudo–deposition term with loss rate 5×10^{-2} $\mathrm{s^{-1}}$ dramatically worsened the model–measurement agreement for other compounds such as MPAN and PAN while only partially reducing the over–prediction of glyoxal. Another possibility which could reduce the modeled glyoxal concentration without disturbing global photochemistry is to reduce the branching ratio of the glycolaldehyde + OH reaction, which is 0.29 in the base–case model and 0.20 in the unaltered MCM. Because glycolaldehyde + OH is the dominant model production pathway for glyoxal at the site ($>$90%), the concentration of glyoxal depends nearly linearly on this branching ratio. The results of a sensitivity analysis on the yield of glyoxal from glycolaldehyde ($\alpha_{\mathrm{glycolaldehyde}\rightarrow\mathrm{glyoxal}}$) using the AB+ basis set are presented in Fig. 9. The top panel shows the model overprediction at two different times of day, indicating that a value of $\alpha_{\mathrm{glycolaldehyde}\rightarrow\mathrm{glyoxal}} \sim 0.045$ is required to match model to measurement. The bottom panel shows the diurnal profiles of modeled and measured glyoxal, with lines indicating the two points in time where ratio were taken. The inferred production yield falls substantially below literature yields of glyoxal to glycolaldehyde, which range from 0.14 to 0.29 (e.g., Magneron et al., 2005; Butkovskaya et al., 2006; Chan et al., 2009). To the authors' knowledge, there is no known process which could reduce the yield of glyoxal from glycolaldehyde to this extent.

References

Bouvier-Brown, N. C., Goldstein, A. H., Worton, D. R., Matross, D. M., Gilman, J. B., Kuster, W. C., Welsh-Bon, D., Warneke, C., de Gouw, J. A., Cahill, T. M., and Holzinger, R.: Methyl chavicol: characterization of its biogenic emission rate, abundance, and oxidation products in the atmosphere, Atmos. Chem. Phys., 9, 2061, 2009.

Butkovskaya, N. I., Pouvesle, N., Kukui, A., and Le Bras, G.: Mechanism of the OH–Initiated Oxidation of Glycolaldehyde over the Temperature Range 233–296 K, The Journal of Physical Chemistry A, 110, 13 492–13 499, 2006.

Chan, A. W. H., Galloway, M. M., Kwan, A. J., Chhabra, P. S., Keutsch, F. N., Wennberg, P. O., Flagan, R. C., and Seinfeld, J. H.: Photooxidation of 2-methyl-3-buten-2-ol (MBO) as a potential source of secondary organic aerosol, Environmental Science and Technology, 43, 4647–4652, doi:10.1021/es802560w, 2009.

Choi, W., Faloona, I. C., McKay, M., Goldstein, A. H., and Baker, B.: Estimating the atmospheric boundary layer height over sloped, forested terrain from surface spectral analysis during BEARPEX, Atmospheric Chemistry and Physics Discussions, 10, 25 759–25 801, 2010.

Day, D. A., Wooldridge, P. J., Dillon, M. B., Thornton, J. A., and Cohen, R. C.: A thermal dissociation laser-induced fluorescence instrument for in situ detection of NO_2, peroxy nitrates, alkyl nitrates, and HNO_3, J. Geophys. Res., 107, 4046, 2002.

DeCarlo, P. F., Kimmel, J. R., Trimborn, A., Northway, M. J., Jayne, J. T., Aiken, A. C., Gonin, M., Fuhrer, K., Horvath, T., Docherty, K. S., Worsnop, D. R., and Jimenez, J. L.: Field-deployable, high-resolution, time-of-flight aerosol mass spectrometer, Anal Chem, 78, 8281–8289, 2006.

Dillon, M. B., Lamanna, M. S., Schade, G. W., Goldstein, A. H., and Cohen, R. C.: Chemical evolution of the Sacramento urban plume: Transport and oxidation, J. Geophys. Res., 107, 2002.

Faloona, I. C., Tan, D., Lesher, R. L., Hazen, N. L., Frame, C. L., Simpas, J. B., Harder, H., Martinez, M., Di Carlo, P., Ren, X., and Brune, W. H.: A Laser-induced Fluorescence Instrument for Detecting Tropospheric OH and HO_2: Characteristics and Calibration, J. Atmos. Chem., 47, 139–167, 2004.

Farmer, D., Kimmel, J. R., Phillips, G., Docherty, K. S., Worsnop, D. R., Sueper, D., Nemitz, E., and Jimenez, J. L.: Eddy covariance measurements with high-resolution time-of-flight aerosol mass spectrometry: a new approach to chemically-resolved aerosol fluxes, Amtos. Measur. Techn. Disc., 3, 5867–5905, 2010.

Farmer, D. K. and Cohen, R. C.: Observations of HNO_3, ΣAN, ΣPN and NO_2 fluxes: evidence for rapid HO_x chemistry within a pine forest canopy, Atmos. Chem. Phys., 8, 3899, 2008.

Galloway, M. M., Huisman, A. J., Yee, L. D., Chan, A. W. H., Loza, C. L., Seinfeld, J. H., and Keutsch, F.: Yields of oxidized volatile organic compounds during the OH radical initiated oxidation of isoprene, methyl vinyl ketone, and methacrolein under high–NO_x conditions, Atmos. Chem. Phys. Disc., p. submitted, 2011.

Gilman, J. B., Burkhart, J. F., Lerner, B. M., Williams, E. J., Kuster, W. C., Goldan, P. D., Murphy, P. C., Warneke, C., Fowler, C., Montzka, S. A., Miller, B. R., Miller, L., Oltmans, S. J., Ryerson, T. B., Cooper, O. R., Stohl, A., and de Gouw, J. A.: Ozone variability and halogen oxidation within the Arctic and sub-Arctic springtime boundary layer, Atmos. Chem. Phys., 10, 10 223–10 236, 2010.

Goldan, P. D., Kuster, W. C., Williams, E., Murphy, P. C., Fehsenfeld, F. C., and Meagher, J.: Nonmethane hydrocarbon and oxy hydrocarbon measurements during the 2002 New England Air Quality Study, J. Geophys. Res., 109, D21 309, 2004.

Goldstein, A. H., Hultman, N. E., Fracheboud, J. M., Bauer, M. R., Panek, J. A., Xu, M., Qi, Y., Guenther, A. B., and Baugh, W.: Effects of climate variability on the carbon dioxide, water, and sensible heat fluxes above a ponderosa pine plantation in the Sierra Nevada (CA), Agric. For. Meteorol., 101, 113, 2000.

LaFranchi, B.: Personal communication regarding the deposition velocity of O_3 in current-generation Berkeley atmospheric models, 2008.

Lee, A., Goldstein, A. H., Kroll, J. H., Ng, N. L., Varutbangkul, V., Flagan, R. C., and Seinfeld, J. H.: Gas-phase products and secondary aerosol yields from the photooxidation of 16 different terpenes, J. Geophys. Res., 111, 2006.

Magneron, I., Mellouki, A., Le Bras, G., Moortgat, G. K., Horowitz, A., and Wirtz, K.: Photolysis and OH–Initiated Oxidation of Glycolaldehyde under Atmospheric Conditions, The Journal of Physical Chemistry A, 109, 4552–4561, 2005.

Orlando, J. J., Tyndall, G. S., Bertman, S. B., Chen, W., and Burkholder, J. B.: Rate coefficient for the reaction of OH with CH2=C(CH3)C(O)OONO2 (MPAN), Atmos. Environ., 36, 1895–1900, 2002.

Perez, I. M., LaFranchi, B. W., and Cohen, R. C.: Nitrogen oxide chemistry in an urban plume: investigation of the chemistry of peroxy and multifunctional organic nitrates with a Lagrangian model, Atmos. Chem. Phys. Disc., 9, 27 099–27 165, 2009.

Ulbrich, I. M., Canagaratna, M. R., Zhang, Q., Worsnop, D. R., and Jimenez, J. L.: Interpretation of organic components from Positive Matrix Factorization of aerosol mass spectrometric data, Atmos Chem Phys, 9, 2891–2918, 2009.

Volkamer, R., San Martini, F., Molina, L. T., Salcedo, D., Jimenez, J. L., and Molina, M. J.: A missing sink for gas-phase glyoxal in Mexico City: Formation of secondary organic aerosol, Geophys. Res. Lett., 34, L19 807, 2007.

Wolfe, G. M., Thornton, J. A., Yatavelli, R. L. N., McKay, M., Goldstein, A. H., LaFranchi, B., Min, K. E., and Cohen, R. C.: Eddy covariance fluxes of acyl peroxy nitrates (PAN, PPN and MPAN) above a Ponderosa pine forest, Atmos. Chem. Phys., 9, 615, 2009.

Table S1. Hot and cold period correlations (half–hourly data points)

Hot Period			Cold Period		
Molecule	Num. Points	R^2	Molecule	Num. Points	R^2
MPAN	362	0.59	MVK	332	0.45
MVK	671	0.41	isoprene	332	0.37
isoprene	671	0.27	MPAN	170	0.31
PPN	362	0.27	MBO	332	0.22
benzene	671	0.20	methyl chavicol	143	0.20
CO	715	0.18	HOA	71	0.15
toluene	671	0.14	toluene	332	0.13
TOA	279	0.09	CO	331	<0.05
HOA	270	0.08	TOA	71	<0.05
OOA	279	0.07	OOA	71	<0.05
MBO	671	0.07	β-pinene	332	<0.05
methyl chavicol	248	<0.05	α-pinene	332	<0.05
β-pinene	651	<0.05	PPN	170	<0.05
α-pinene	651	<0.05	benzene	332	<0.05

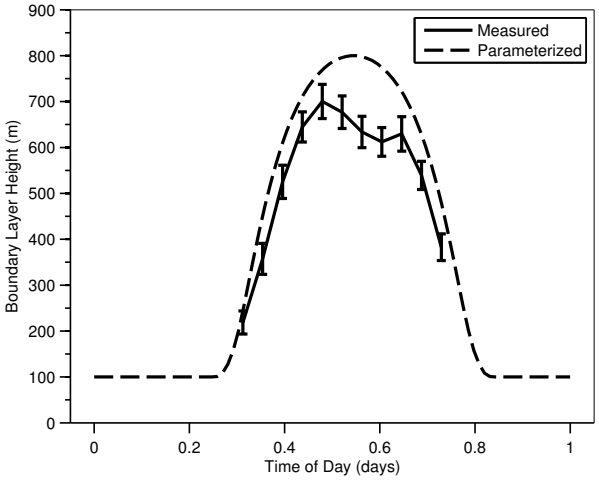

Fig. S1. Measured and parameterized boundary layer height. Measurements are the average of available hot period data, and error bars reflect the variability in data, not reported uncertainty.

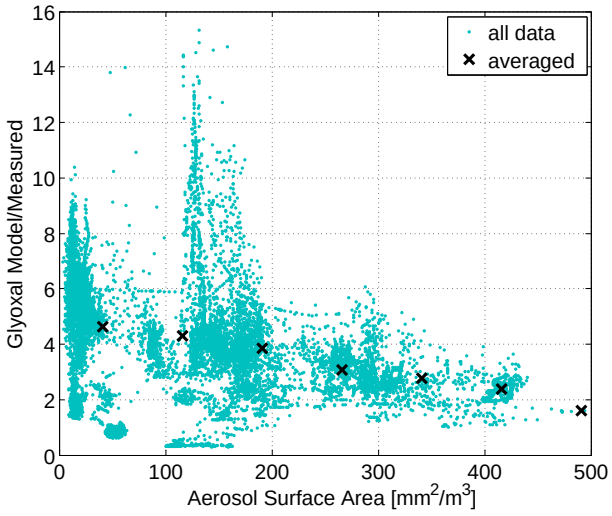

Fig. S2. Ratio of modeled to measured glyoxal as a function of aerosol surface area for model runs with no aerosol loss term for glyoxal. If aerosol loss corresponds to an important sink of glyoxal, model-measurement agreement should degrade at high aerosol surface areas. This is not the case, which shows that aerosol loss was not an important glyoxal sink during BEARPEX 2007. The analysis of daytime only values (not shown) produces the same result.

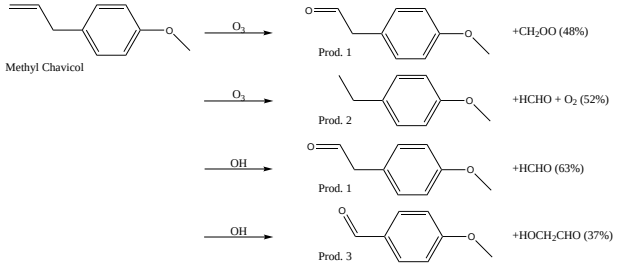

Fig. S3. Mechanism for OH and O_3 degradation of methyl chavicol. Glycolaldehyde (here denoted HOCH2CHO) is produced by the minor channel of OH–initiated oxidation. Mechanism from Bouvier-Brown et al. (2009) and branching ratios from Lee et al. (2006).

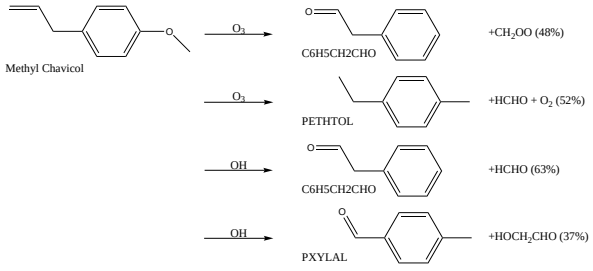

Fig. S4. MCM-based implementation of pseudo–methyl chavicol degradation mechanism. Structural analogs for the true products (cf. Fig. S3) which are already in place in the MCM are used without altering the other products or branching ratios.

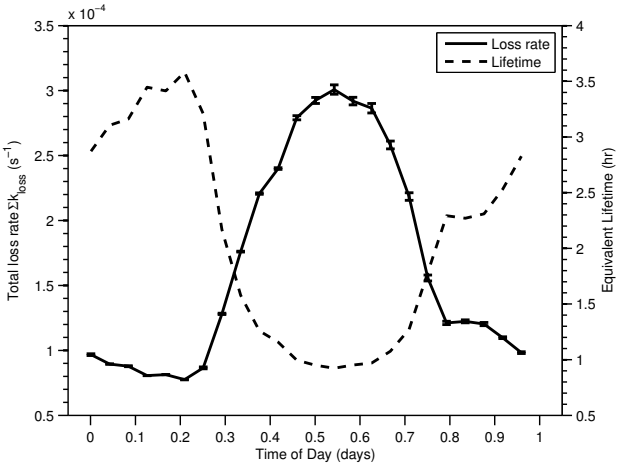

Fig. S5. Diurnal profile in calculated loss rates for glyoxal and equivalent lifetime in hours for BFRS for the full chemistry basis set. The nighttime loss rate is dominated by deposition and OH oxidation, while daytime loss rates are driven by photolysis and OH. The short lifetime of glyoxal, especially during the day, enables the use of the 0–D box model for comparisons as reduces the importance of transport of glyoxal.

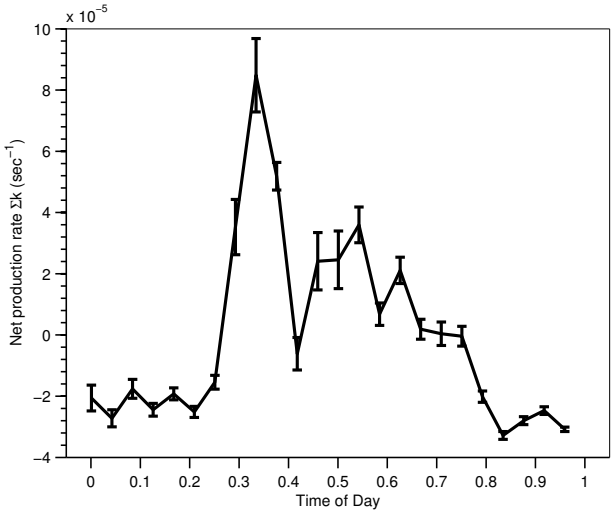

Fig. S6. Diurnally averaged net production rate of glyoxal calculated by model using isoprene and MBO, with downstream oxidation products, as source molecules. The production rate should be comparable to the fitted loss rate used in the nighttime deposition analysis in Sect. 3.2. The large spike in net production rate corresponds roughly to the morning increase in MBO and OH.

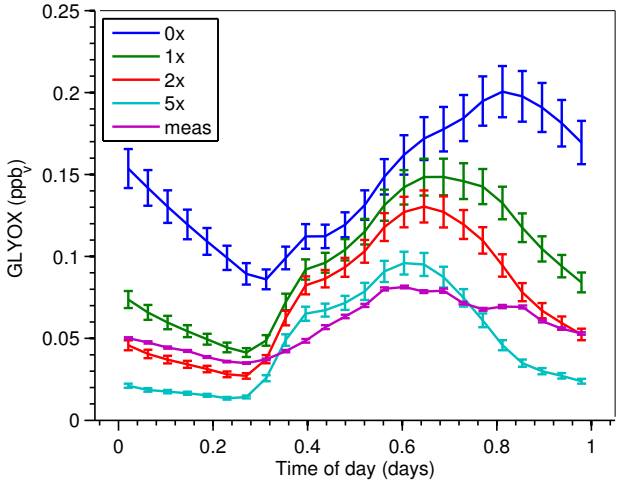

Fig. S7. Diurnal profile of modeled glyoxal using different multipliers of uptake coefficient γ and diurnally averaged aerosol surface area, indicated by the legend. A run with no aerosol (0x) has substantially more glyoxal, especially at night. An enhancement of $\sim$5 in γ is required to bring daytime glyoxal into agreement with model, resulting in a distortion of the diurnal cycle. In addition the variability in high and low aerosol surface areas introduces significant excursions from this average, with low–aerosol days experiencing too little loss and high–aerosol days experiencing too much loss.

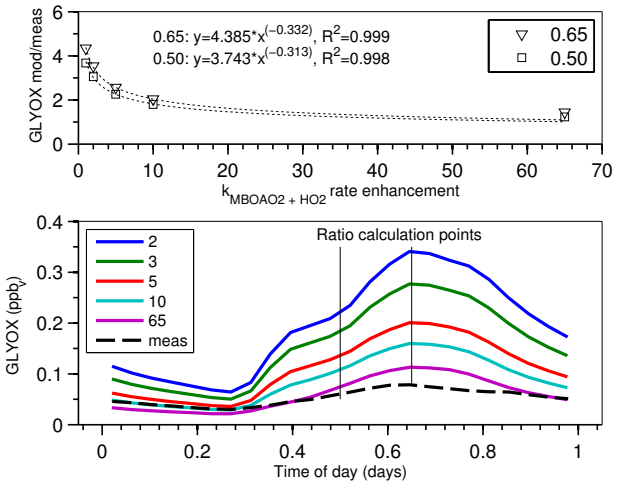

Fig. S8. Top panel: model over–prediction of glyoxal at 0.65 day and 0.50 day as a function of the rate constant for MBOAO2 + HO_2 reaction, fit to a power–law. The time at which the ratio was calculated is indicated in the legend. An enhancement of over 60–fold in the rate is required to reduce the model to measured values. Bottom panel: diurnal average profiles of measured glyoxal and the model runs depicted in the top panel. The legend indicates the enhancement in MBOAO2 + HO_2 reaction rate, and vertical lines indicate the point in time where ratios were calculated.

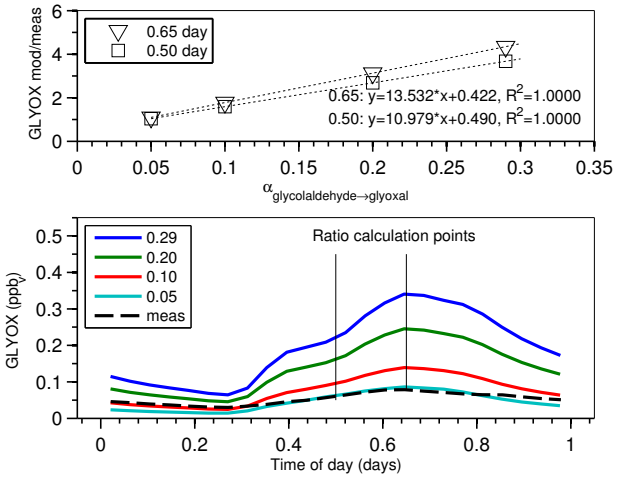

Fig. S9. Top panel: model over–prediction of glyoxal at 0.65 day and 0.50 day as a function of the branching ratio of glycolaldehyde + OH to glyoxal, $\alpha_{\text{glycolaldehyde}\rightarrow\text{glyoxal}}$, fit to a line. This experiment indicates a branching ratio of 0.035 is needed to match models to measurement. Bottom panel: diurnal average profiles of measured glyoxal and the model runs depicted in the top panel. The legend indicates the branching ratio, and vertical lines indicate the point in time where ratios were calculated.